# In-Situ X-ray Scattering Studies of a Unique Toughening Mechanism in Surface-Modified Carbon Nanofiber/UHMWPE Nanocomposite Films

**Xuming Chen, Kyunghwan Yoon, Christian Burger, Igors Sics, Dufei Fang, Benjamin S. Hsiao,* and Benjamin Chu***

*Department of Chemistry, State University of New York at Stony Brook, Stony Brook, New York 11794-3400*

*Received October 1, 2004; Revised Manuscript Received January 11, 2005*

ABSTRACT: The toughening mechanism of nanocomposite films comprising ultrahigh molecular weight polyethylene (UHMWPE) and modified carbon nanofiber (MCNF) was investigated by in-situ synchrotron small-angle X-ray scattering (SAXS) and wide-angle X-ray diffraction (WAXD) techniques during uniaxial stretching. Surface modification of carbon nanofibers included oxidation and subsequent chemical reaction with octadecylamine. At room temperature, the toughness of melt-pressed nanocomposite films was found to increase over 10 times by addition of 0.2 and 5 wt % of MCNF compared to that of pure UHMWPE. WAXD and SAXS results indicated that MCNF acted as a solvent carrier in the stiff UHMWPE matrix, whereby the grafted short hydrocarbon chains ($n = 18$) plasticized the surrounding UHMWPE chains in the nanoscale vicinity (10−20 nm) and induced interfacial flow under stretching, resulting in a large elongation-to-break ratio (>500%). A martensitic crystal transformation in UHMWPE was detected in all samples during deformation, where the transformation mode could be assigned as $T_{12}$. At high temperature (118 °C), the toughness of the MCNF/UHMWPE composite films was still about 2 times higher than that of pure UHMWPE. The mobile hydrocarbon layers at the UHMWPE/MCNF interface appeared to be the key to overcome the barrier of high chain entanglements in the solid UHMWPE matrix and to induce the significantly toughened performance.

## Introduction

Recently, the family of carbon nanotubes, including single-wall nanotube (SWNT), multiwall nanotube (MWNT), and carbon nanofibers (CNFs),[1−3] has received a great deal of attention in the polymer community. These nanostructured materials have been recognized for their superior mechanical strength, excellent thermal conductivity, and electrical conductivity.[4] Frequently, they are used as nanofillers to improve the polymer properties. In the case of mechanical enhancement, all published work on polymeric nanocomposites containing carbon nanotubes indicated that the improvement, although notable, is only incremental,[5−11] substantially below the expectation of the super-tough performance of poly(vinyl alcohol) (PVA)/SWNT nanocomposite fibers demonstrated by Dalton et al.[12] In their study, the unusually high elongation-to-break ratio in SWNT/PVA fiber appeared to be the key to the super-tough property. They attributed this behavior to the extension of amorphous PVA chains between SWNTs during deformation, similar to the extension of protein chains in the amorphous domains between relatively rigid crystalline regions in spider silk.

Inspired by the work of Dalton et al.,[12] our laboratory has also explored a different pathway to prepare significantly toughened polymeric nanocomposites containing surface-modified carbon nanotubes and stiff polymer matrices in this study. CNF has been chosen as the nanofiller for the following reasons. (1) CNFs can be mass-produced by the vapor growth method,[13] and are significantly cheaper than SWNTs or multiwall nanotubes (MWNTs). (2) CNFs also have an exceedingly high anisotropic shape with an average diameter of 50−200 nm, bridging the gap between the size of conventional carbon fibers (7−10 $\mu$m) and those of SWNTs (a few nanometers) and MWNTs (a few tens of nanometers). (3) The surface modification of CNFs, typically involving two steps—oxidation and subsequent grafting of long hydrocarbon chains on the CNF surface—is very straightforward and easier than those of SWNTs and MWNTs.

In this study, modified carbon nanofiber (MCNF) serves as a solvent carrier in the composite. In other words, the short hydrocarbon chains on the surface of MCNF can act as solvent molecules to the polymer matrix chains. Although MCNF may not change too much about the modulus and the strength of the matrix, it can significantly increase the elongation-to-break ratio and therefore the toughness. This makes the function of MCNF very different from that of carbon nanotubes (CNF) in conventional polymer nanocomposites.[5−11] However, we speculate that this pathway may only be effective to toughen the stiff polymer matrix, where the stiffness is due to the high entanglement density. If the matrix is not stiff (e.g., semicrystalline polymers of low entanglement density), the toughness improvement by adding MCNF may be limited and probably through a different mechanism.

The chosen matrix was UHMWPE, which was selected for the following reasons. First, the UHMWPE matrix is known to have a very low elongation-to-break ratio due to the high entanglement density; thus, it fits the requirement of a stiff matrix. Second, we intend to develop a process to produce toughened UHMWPE films or fibers without the use of solvent in the end processing step. The development of high-performance UHMWPE films and fibers has been well established in industry and academia[14−17] and often involved the use of a low molecular weight solvent to reduce the high entangle-

* To whom correspondence should be addressed: Tel (631) 632-7793 (Hsiao), (631) 632-7928 (Chu); Fax (631) 632-6518; e-mail bhsiao@notes.cc.sunysb.edu (Hsiao), bchu@notes.cc.sunysb.edu (Chu).

10.1021/ma047978r CCC: $30.25 
Published on Web 04/02/2005

ment density when forming the final products. For example, Smith and Lemstra successfully demonstrated the techniques of film drawing and fiber-spinning in the gel state.[15] The UHMWPE gel film or gel fiber has a very high draw ratio, which can result in very high modulus and tensile strength. The key feature of these techniques is the use of a relatively good solvent to prepare a less entangled polymer network for processing, followed by solidification and removal of the solvent. Recently, Bin et al. demonstrated that UHMWPE gel films could be stretched to a high draw ratio, normally above 100.[11] The resulting polyethylene chains were highly elongated; the final polymer matrix exhibited a very high degree of crystallinity and excellent mechanical properties. However, if processed by melt-processing without the aid of solvent, UHMWPE chains usually possess an extraordinarily high entanglement density, leading to very low draw ability and brittleness in the final product. For example, in a study of compression-molding of UHMWPE reactor powder, Nakae et al. reported that the different level of entanglement formation (being associated with the scale of segmental diffusion) affected the resultant structure and the draw ability of UHMWPE significantly.[18,19]

In this study, we demonstrate that the surface-modified carbon nanofiber (MCNF) is the key for the preparation of significantly toughened nanocomposites based on ultrahigh molecular weight polyethylene (UHMWPE). We hypothesize that the presence of short hydrocarbon chains on the MCNF surface plasticizes the long UHMWPE chains in the fiber/matrix interface, thus resulting in an interfacial flow under stretching and enhancing the elongation-to-break ratio. This hypothesis was confirmed by in-situ small-angle X-ray scattering (SAXS) and wide-angle X-ray diffraction (WAXD) studies of the MCNF/UHMWPE nanocomposite during deformation using synchrotron radiation. No significantly toughened performance was observed in the CNF/UHMWPE nanocomposite, where the surface of CNF was not modified.

## Experimental Section

The UHMWPE sample (1900 H), which had a weight-average molecular weight ($M_w$) of $6 \times 10^6$ g/mol and a polydispersity of about 9, was provided by Basell. The carbon nanofiber (PR-24-HHT) was obtained from Pyrograf Products, Inc., without further purification. The surface modification of CNF was carried out as follows. The acidic groups (carboxylic acid and hydroxyl) on the carbon nanofiber (CNF) surface were generated by an oxidation reaction using potassium chlorate/sulfuric acid solution.[20] The amount of carboxylic acid group on the surface of oxidized CNF was determined by titration using $NaHCO_3$ solution.[21] The oxidized CNFs were then dispersed in octadecylamine, which was maintained at 180−200 °C under nitrogen for 20 h. The resulting suspension was filtered, washed with THF and then with hexane, and subsequently dried in vacuo at 70 °C. The degree of modification was checked with Raman spectroscopy and thermal gravimetric analysis (TGA). The Raman spectra of the as-received CNF, oxidized CNF, and MCNF were collected using the Renishaw 2000 spectrometer with a 500 mW, 785 nm HPNIR785 laser (Renishaw Inc., U.K.). The TGA scans of CNF, oxidized CNF, and MCNF were collected at 20 °C/min by using TGA 7 from Perkin-Elmer Inc.

For nanocomposite preparation, MCNFs were first added to decalin to form a uniform suspension under ultrasonic vibration at room temperature. The MCNF suspension was subsequently added to a 1 wt % UHMWPE/decalin solution. The MCNF/UHMWPE/decalin mixture was then heated to 130−140 °C for 90 min under vigorous stirring and formed a homogeneous suspension. Upon being cooled to room temperature, decalin was extracted from the suspension. The sample was then melt mixed with 0.5 wt % (based on the amount of UHMWPE) of antioxidant 3-(3,5-di-*tert*-butyl-4-hydroxy)phenyl propanate using a twin-screw blender (DACA Instruments) at 170 °C for 5 min to prevent thermal degradation. The recovered sample was dried in a 60 °C oven to constant weight. Three nanocomposite samples were prepared for this study, having the amounts of MCNF as 0.0, 0.2, and 5.0 wt %. For comparison purposes, a nanocomposite sample containing 0.2 wt % of oxidized CNF but with no further modification was also prepared using the same procedure. All samples were melt-pressed into flat films (with a thickness of about 0.2 mm) under the following conditions: the temperature was 180 °C, the pressure was 2.1 MPa, and the hold time was 5 min, followed by quenching in ice water. The surface and the cross-section views of the nanocomposite film were examined by scanning electron microscopy (SEM, LEO1550, LEO). The cross-section view of the fibers was obtained by fracturing the nanocomposite films in liquid nitrogen. DSC measurements were carried out in a TA Instrument DSC 7. All samples were heated at 10 °C/min up to 200 °C and then cooled at the same rate, under a nitrogen gas flow. The degree of crystallinity in each sample was calculated using the measured heat of fusion, assuming the heat of fusion for perfect PE crystals (100% crystallinity) is equal to 290 J/g.[22]

In-situ wide-angle X-ray diffraction (WAXD) and small-angle X-ray scattering (SAXS) experiments were carried out at the Advanced Polymers Beamline (X27C) in the National Synchrotron Light Source (NSLS), Brookhaven National Laboratory (BNL). The details of the experimental setup at the X27C beamline have been reported elsewhere.[23] The wavelength used was 0.1366 nm. A three-pinhole collimation system was used to define the incident beam from a double-multilayered monochromator. The sample-to-detector distance for WAXD was 117.8 mm, and that for SAXS was 1890.8 mm. A MAR-CCD (MAR, Inc.) two-dimensional X-ray detector was used for the real-time data collection. A typical image acquisition time was 15 s per image. The sample was uniaxially stretched using a modified Instron 4442 tensile apparatus, where symmetric deformation was carried out. The initial length between the Instron jaws was 10 mm. The experiments were carried out at room temperature and at high temperature (118 °C) using an environmental chamber. In-situ WAXD and SAXS measurements during stretching were carried out separately for each film sample. The chosen stretching rate was 5 mm/min. The crystallinity change was also estimated from the WAXD pattern. 2D WAXD patterns were corrected for the effects of the curvature of the Ewald sphere (Fraser correction[24]). The integrated peak intensity for each selected strong crystal reflection and the amorphous background were extracted by a curve-fitting program.[21] The crystallinity was calculated as the ratio of the total crystal peak intensity to total diffraction intensity. Hermans' orientation factors $\bar{P}_2$ were calculated from the equatorial peaks, separately for the various phases. In the SAXS analysis, the total integrated intensity was also calculated using a custom program,[24] which was proportional to the scattering invariant.

## Results and Discussion

**Surface Modification of CNF and Characterization of MCNF/UHMWPE Nanocomposites**. The as-received CNF sample was thermally treated to remove the non-carbon compounds. It had an average diameter of 100 nm and a length of 50−100 $\mu$m (Figure 1). The surface modification of CNF involved two processes: (1) surface oxidation using potassium chlorate/sulfuric acid solution[20] and (2) grafting reaction with octadecylamine (number of carbons = 18). The amount of carboxylic acid group on the CNF surface after oxidation was determined by the titration method. Typically, after 4 days of oxidation, the carboxylic acid value on the CNF surface was 0.76 mmol/(g of CNF), corresponding to a

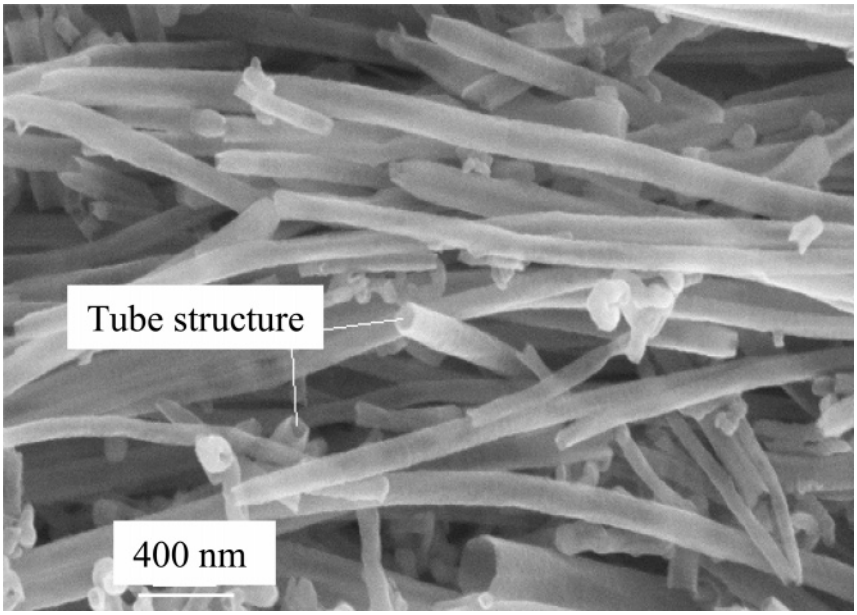


**Figure 1.** Typical SEM image of the as-received CNF sample.

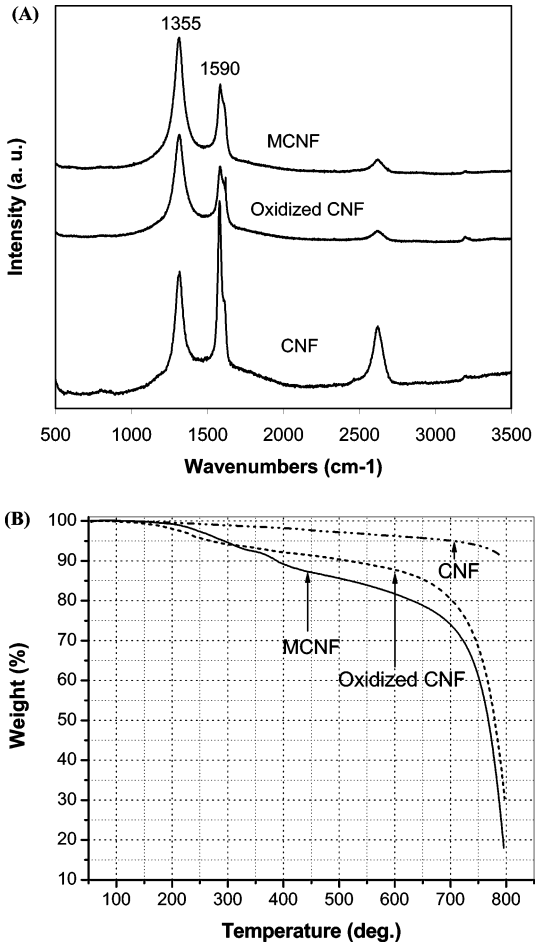


**Figure 2.** Raman spectra (A) and TGA thermograms (B) of CNF, oxidized CNF, and MCNF.

level that every 109 carbon in the CNF (in bulk) had one carboxylic acid group that was grafted.[25] The Raman spectra of CNF, oxidized CNF, and MCNF were measured to determine the degree of surface modification. In the Raman spectra (Figure 2A), the ratio (ID/IG) can be taken as a measure of the crystalline order in the graphitic system, where ID represents the intensity of the disordered band (D-band) at 1355 $cm^{-1}$ and IG represents the intensity of the graphitic band (G-band) at 1590 $cm^{-1}$. A small ID/IG ratio would indicate few defects, a small amount of amorphous carbon, and high graphitic order on the surface. It was found that after oxidation the ID/IG ratio increased from 0.73 to 1.3, indicating that the crystalline order of graphite on the CNF surface decreased. The ID/IG ratio of MCNF was 1.4, suggesting that the amidation reaction did not further change the CNF surface. The thermal stability of MCNF was tested by thermogravimetric analysis (TGA). The as-received CNF exhibited a higher thermal stability than that of oxidized CNF and MCNF. In MCNF, a distinct weight loss in the range of 300−400 °C, corresponding to the decomposition of octadecylamide molecules, was seen. The weight difference between oxidized CNF and MCNF was about 5% (Figure 2B). This result indicated that only about 30% of carboxylic acid groups on the surface of MCNF were converted to octadecylamide groups (i.e., 70% of carboxylic acid groups were not grafted with octadecylamine).

In nanocomposites, the dispersion of MCNF in UHMWPE was extremely good, even when the MCNF content was increased to 5 wt %. For example, SEM examination of the cryogenically fractured nanocomposite film containing 5 wt % MCNF did not show any sign of MCNF aggregation in the UHMWPE matrix, and the interfacial adhesion between MCNF and UHMWPE was found to be excellent. (A typical SEM image of the fractured 5 wt % MCNF nanocomposite sample is shown in Figure 3.)

**Toughening Performance at Room Temperature.** For each prepared film sample, three tensile specimens were tested for mechanical evaluation, and all stress−strain curves were found to be similar. The typical stress−strain curves of neat UHMWPE, oxidized CNF/UHMWPE, and MCNF/UHMWPE (with 0.2 and 5 wt % MCNF) films are shown in Figure 4. It is noted that the initial moduli of these samples were about the same, but both MCNF/UHMW nanocomposite films exhibited significant increases in the elongation-to-break ratio (ca. 10 times more than that of neat

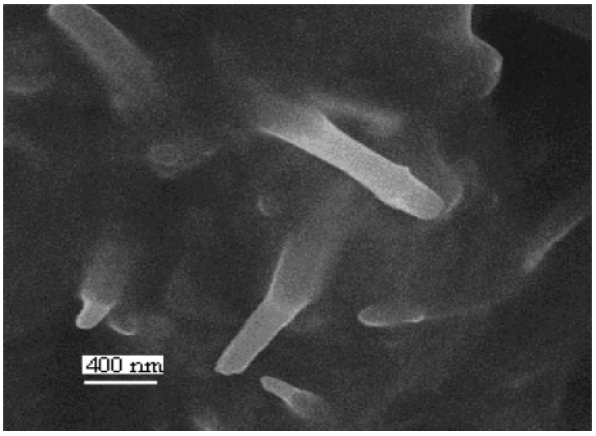


**Figure 3.** Typical SEM image of cross-sectioned MCNF/UHMWPE nanocomposite film containing 5 wt % MCNF.

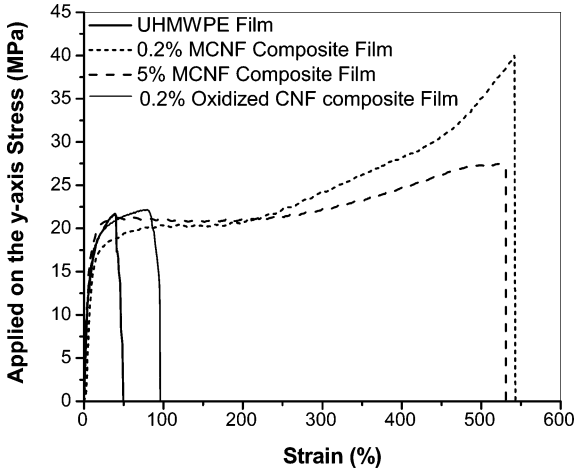


**Figure 4.** Stress−strain curves of the melt-pressed UHMWPE, oxidized CNF/UHMWPE, and MCNF/UHMWPE (with 0.2 wt % MCNF and 5 wt % MCNF) films.

UHMWPE). The 0.2 wt % oxidized CNF film also showed an increase in the elongation-to-break ratio (ca. 2 times more than that of neat UHMWPE), but substantially less that that of MCNF/UHMWPE. The performance of the 0.2 wt % MCNF sample was most unexpected and also exhibited the highest value of ultimo-tensile strength. If one used the integrated area under the stress and strain curve to gauge the toughness of the film, then the toughness values of the 0.2 and 5 wt % MCNF films were about 16 and 14 times that of the pure UHMWPE film and about 7 and 6 times that of the 0.2 wt % oxidized CNF film, respectively. This observation indicates the significantly toughened performance in the MCNF/UHMWPE nanocomposite, even though the tested system was not fully optimized. The similar moduli data measured in UHMWPE and MCNF/UHMWPE films indicated that the addition of MCNF in UHMWPE did not exhibit a typical filler reinforcement effect. One would expect the modulus of the nanocomposite to be higher than that of the neat resin because the modulus of MCNF is about 600 GPa [26] and the modulus of polyethylene extended chain crystals is 240−340 GPa.[27] However, this was not seen. The substantial improvement of the toughness cannot be explained by the conventional stress field theories for the filled polymers, based on stress field overlap and/or transitions of the stress state developed for the filled polymers.[28]

**Table 1. Melting Temperature and Crystallinity of UHMWPE and MCNF/UHMWPE Nanocomposite Films Determined by DSC**

| MCNF concentration (%) | 0 | 0.2 | 5 |
|---|---|---|---|
| melting point (°C) | 133.6 | 132.9 | 132.1 |
| $\Delta H_f$ (J/g) | 110.3 | 115.2 | 115.0 |
| $\Delta H_f$ (J/g)[a] | 110.3 | 115.4 | 121.0 |
| crystallinity (%) | 38.0 | 39.7 | 39.8 |

[a] Do not consider the weight of MCNF.

The brittleness of the pressed UHMWPE film can be attributed to the low elongation-to-break ratio. It is reasonable to assume that the hot-press process at 180 °C, which is about 40 °C above the equilibrium melting temperature of PE,[19] generated a great deal of chain entanglements, which severely hindered the draw ability of the final sample at room temperature. This argument is consistent with the DSC data (Table 1), where the crystallinity ($X_c$) of the pressed sample (~54%) was much lower than that of the as-polymerized sample (~80%). This is not surprising since the high chain entanglements in melt-processed UHMWPE can suppress the crystallization process and result in lower crystallinity. In the MCNF/UHMWPE samples, the crystallinity was found to be even lower (41% for the 0.2 wt % MCNF sample and 38% for the 5 wt % MCNF sample). This would indicate that, should the chain entanglement density further increase, it could lead to a lower elongation-to-break ratio. However, this was opposite to our results. Therefore, the much improved elongation-to-break ratio in the MCNF/UHMWPE nanocomposites must be due to some other factors, which overcome the barrier of high entanglement in UHMWPE.

**Wide-Angle X-ray Diffraction Characterization.** The toughness improvement of the MCNF/UHMWPE nanocomposites can be indirectly probed by monitoring the crystal structural changes in UHMWPE during stretching using in-situ synchrotron wide-angle X-ray diffraction (WAXD) techniques. From the 2D WAXD data, a crystal martensitic transformation,[29] corresponding to the conversion of orthorhombic to monoclinic crystal structure in PE, was seen in both nanocomposite samples. A typical 2D WAXD pattern of the stretched 5 wt % MCNF nanocomposite (strain at 208%) containing both orthorhombic and monoclinic structures is shown in Figure 5A, where the (200) and (110) reflections of the orthorhombic phase and the (010), ($\bar{2}$10), and (200) reflections of the monoclinic phase are indexed. (Based on the literature data, the unit cell parameters for the monoclinic phase are $a = 8.09$ Å, $b = 4.79$ Å, $c = 2.54$ Å, and $\gamma = 107.9°$, where the unit cell parameters for the orthorhombic phase are $a = 7.42$ Å, $b = 4.95$ Å, and $c = 2.54$ Å. [31]) The monoclinic phase in PE has been shown to be metastable, existing only under stress and below 110 °C.[29,30] The monoclinic phase often appears during melting of oriented PE samples with intermediate molecular weights, but it has not been observed in oriented UHMWPE gel films,[11,16] which is probably due to the very low entanglement of the polymer chains in the gel state. As the chain entanglement in the hot-pressed UHMWPE film was extraordinarily high, it is understandable that both orthorhombic and monoclinic structures can coexist under the elongation process. Corresponding $d$ spacings of observed crystal peaks from both crystal phases are listed in Table 2. In Figure 5A, a relatively azimuthal independent diffraction ring located at $2\theta$ of 23.2° ($d$

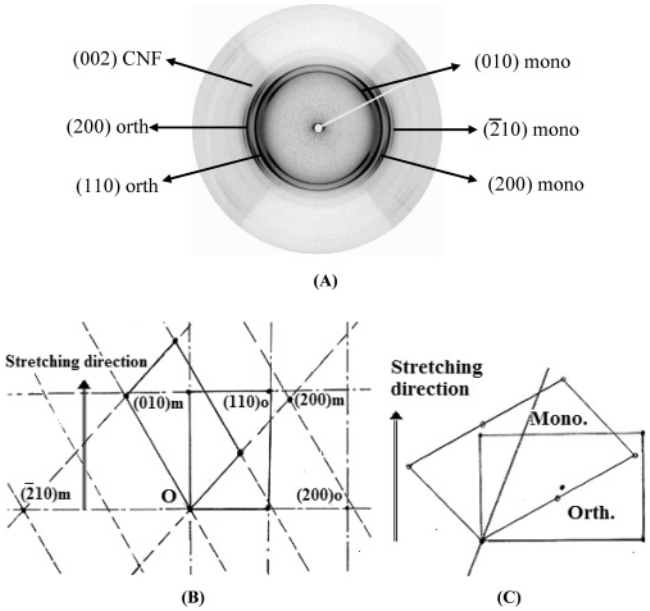


**Figure 5.** 2D WAXD pattern of 5 wt % MCNF nanocomposite film under stretching at a strain of 208% (A) and schematic representation mode of martensitic transformation of MCNF/UHMWPE composite film (monoclinic cell of polyethylene projected on (001) plane; (B) in reciprocal space, and (C) in real space).

**Table 2. Values of 2$\theta$ and $d$ Spacing of Crystal Diffraction Peaks from 2D WAXD**

| peaks | 1 | 2 | 3 | 4 | 5 | 6 |
|---|---|---|---|---|---|---|
| $d$ (Å) | 4.591 | 4.146 | 3.862 | 3.720 | 3.535 | 3.414 |
| ($hkl$) mono | 110 | | 200 | | $\bar{2}$01 | |
| ($hkl$) orth | | 110 | | 200 | | |
| ($hkl$) CNF | | | | | | 002 |

spacing = 0.34 nm) is also seen. This diffraction is attributed to the interlayer reflection from the graphene layer stacking within the CNF and is thus assigned as the (002) peak of CNF.

It is well-known that in PE the stable orthorhombic phase can be transformed into the metastable monoclinic phase by stress.[29,30] This process is called martensitic transformation. Bevis and Crellin reported all possible modes of martensitic transformation in PE and reduced them to four principal modes: $T_{11}$, $T_{12}$, $T_{21}$, and $T_{22}$.[32] Based on the schematic representation of the transformation mode illustrated in Figure 5B (in reciprocal space) and Figure 5C (in real space), the observed martensitic transformation in the 2D WAXD patterns of MCNF/UHMWPE nanocomposite film exhibited the $T_{12}$ mode. We believe that this crystal transformation is directly resulted from the large strain deformation in the noncrystalline phase, which will be discussed later.

The 2D WAXD data were analyzed to determine the total degree of crystallinity and the corresponding mass fractions of monoclinic and orthorhombic phases in 0.2 and 5 wt % MCNF nanocomposite films. Results are shown in Figure 6, which can be directly related to the significantly toughened performance of the nanocomposite. It is seen that the total crystallinity was relatively low (around 40%) in both initial nanocomposite samples, which were dominated by the stable orthorhombic phase. At strains below 125%, the total crystallinity and the fraction of the orthorhombic phase decreased rapidly during deformation, while the fraction of the monoclinic phase increased accordingly. This

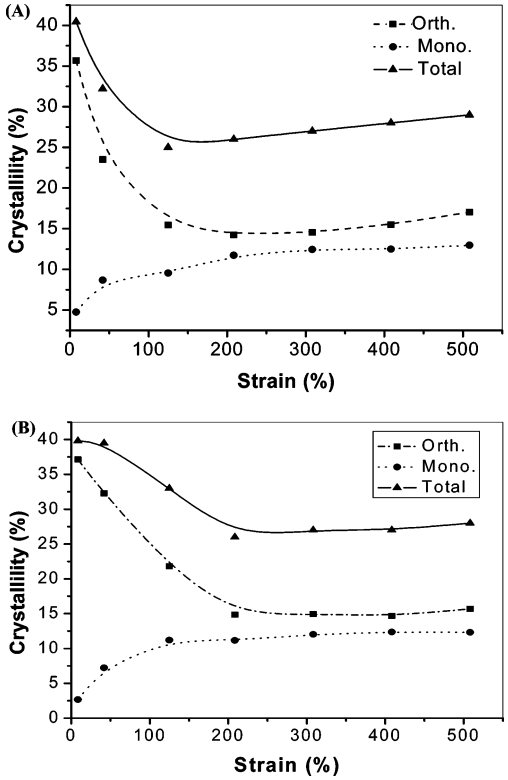


**Figure 6.** Changes of crystallinity fractions of monoclinic and orthorhombic phases as well as of total crystallinity during stretching of 0.2 wt % MCNF (B) and 5 wt % MCNF (C) films.

indicates that some polyethylene chains in the orthorhombic crystal were pulled out (crystallinity reduction), and some were converted into the monoclinic phase by minimal lattice movement (martensitic transformation). The destruction of the initial crystallites (dominated by the orthorhombic phase) was greater than the formation of the new crystallites (dominated by the monoclinic phase). At strains above 200%, a slight increase in the total crystallinity was seen in both samples, indicating that the strain-induced crystallization took place, which was also consistent with the observation of strain-hardening behavior seen in Figure 4.

It is interesting to note that, at the initial stretching stage, the total crystallinity in the 5 wt % MCNF film (Figure 6A) decreased at a much slower rate than that in the 0.2 wt % film (Figure 6B). This indicates that the processes of crystal destruction (via chain pull-out) and re-formation (or martensitic transformation) in the 5 wt % sample were retarded, probably due to the greater extent of the interfacial flow under stretching. As the initial nanocomposite samples were randomly oriented, the stretching deformation would induce the following processes: (1) reorientation of MCNF and PE crystals and (2) destruction and re-formation of PE crystals. It appears that the high extent of interfacial flow around the MCNF greatly facilitates the plastic flow behavior of the 5 wt % sample at the initial deformation process, but the high concentration of MCNF also hinders the total extension of the sample, which is expected from the typical filler effect due to the particulate interactions. In contrast, a small addition of MCNF (0.2 wt %) of UHMWPE was found to simultaneously improve the elongation-to-break ratio (>10 times increase—from 50% to 500%) and the tensile strength (about 2 times increase), which is completely unexpected.

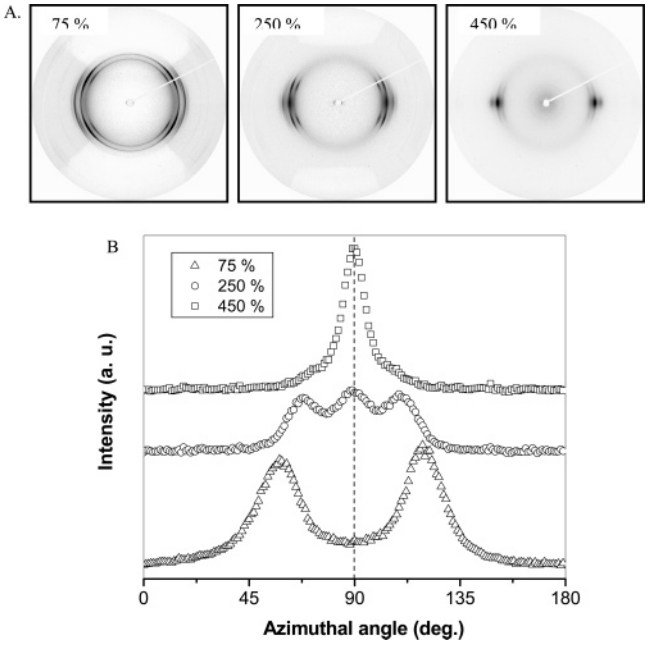


**Figure 7.** (A) WAXD patterns of the 0.2 wt % MCNF film at strains of 75%, 250% and 450%. (B) Corresponding azimuthal profiles of the (110) orthorhombic reflection (the azimuthal angle of the equator is 90°).

The significantly toughened behavior can also be probed from the changes of the crystal orientation during stretching. For example, the shape of the orthorhombic (110) reflection in Figure 5A (at a strain of 208%) showed a four-point pattern instead of two equatorial arcs, indicating the presence of *a*-axis orientation;[33] i.e., the crystallographic *a*-axis is preferentially oriented perpendicular to the fiber axis, and the *b*- and *c*-axis are distributed in a rotationally symmetric way, normal to the *a*-axis. The situation for the monoclinic polyethylene in this regime is similar, but with the $(\bar{2}10)$-axis replacing the *a*-axis of the orthorhombic cell as the perpendicular symmetry axis. Note that in either case the polymer chains, being parallel to the *c*-axis of their unit cells, are not preferentially aligned in the stretching direction. At large strains, this is of course not the expected configuration. Figure 7 illustrates selected WAXD patterns of 0.2 wt % MCNF films at strains of 75%, 250%, and 450% and the corresponding azimuthal profiles of the (110) orthorhombic reflection. It is seen that at the 450% strain all (*hk*0) reflections are found to aggregate on the equator, indicating the expected *c*-axis orientation. The six-point pattern observed at strain of 250% (Figure 7A) indicates the presence of a mixture of *a*-axis and *c*-axis orientation.

The evolution of this orientational transformation can be quantified by following the strain dependence of Hermans' orientation parameter, $\bar{P}_2 = \{(3\langle\cos^2\phi\rangle - 1)/2\}$, where $\bar{P}_2$ is defined by the orientation distribution function (ODF) of the primary axis of the crystals (i.e., the *a*-axis of the orthorhombic cell or the $(\bar{2}10)$-axis of the monoclinic cell at low strains or the *c*-axis of either cell at high strains) with respect to the fiber axis. This means that, for *a*-axis or $(\bar{2}10)$-axis orientation, the $\bar{P}_2$ value extracted from an equatorial reflection will be identical to the $\bar{P}_2$ value of the ODF, and it will lie in the range between 0 and −0.5. However, for *c*-axis orientation, the $\bar{P}_2$ value extracted from an equatorial reflection needs to be multiplied by a factor of −2 to yield the true $\bar{P}_2$ value of the ODF (the value thus will be between 0 and 1).

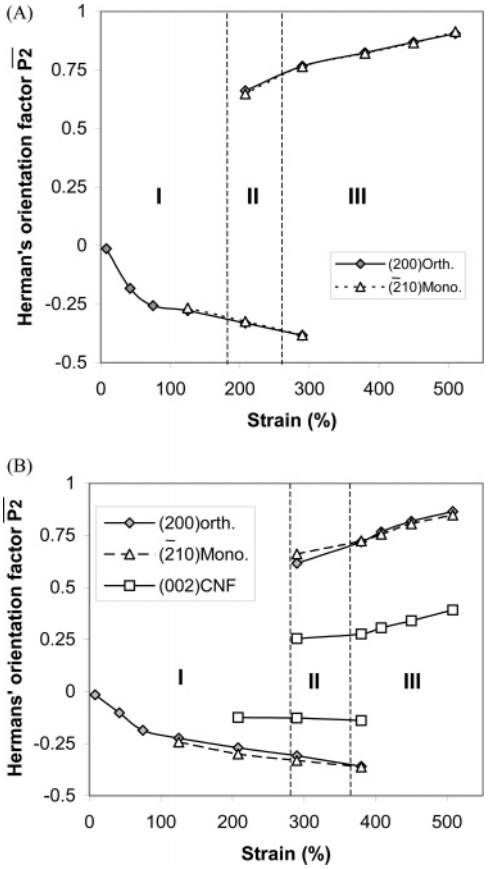


**Figure 8.** Hermans' orientation factor, $\bar{P}_2$, of crystal planes along the *a*-axis and *c*-axis during stretching for (A) 0.2 wt % MCNF film and (B) 5 wt % MCNF film (region I: *a*-axis orientation; region II: both *a*-axis and *c*-axis orientation; region III: *c*-axis orientation).

Figure 8A shows the evolution of Hermans' orientation factor, $\bar{P}_2$, from the (200) reflection of the orthorhombic cell and the $(\bar{2}10)$ reflection of the monoclinic cell for the 0.2 wt % MCNF film during stretching. In general, the $\bar{P}_2$ values from these two reflections of different cells exhibited an excellent agreement, except at the initial deformation stage (strain < 100%), where only the (200) reflection of the orthorhombic cell was seen. Figure 8 can be separated into three regions for discussion. In region I (strain < 200%), there is only the presence of *a*-axis orientation. It is found that the $\bar{P}_2$ value decreases rapidly at strains less than 100% and slowly at strains greater than 100%, indicating the corresponding perfection of the perpendicular *a*-axis orientation. Region II represents the transitional region (strain from 200 to 300%), where both *a*-axis orientation and *c*-axis orientation coexist. The $\bar{P}_2$ value is found to decrease in the *a*-axis orientation and increase in the *c*-axis orientation, suggesting the continuing perfection of these two types of preferred orientation in this region. In region III (strain > 300%), only *c*-axis orientation exists. The corresponding $\bar{P}_2$ value is found to increase steadily, indicating a high degree of preferred orientation of the *c*-axis for both orthorhombic and monoclinic cells with respect to the fiber axis.

Figure 8B shows the $\bar{P}_2$ values for the 5 wt % MCNF film during stretching. Since the (002) reflection of MCNF was strong in the WAXD pattern, the corresponding $\bar{P}_2$ value was calculated. Similar to the above

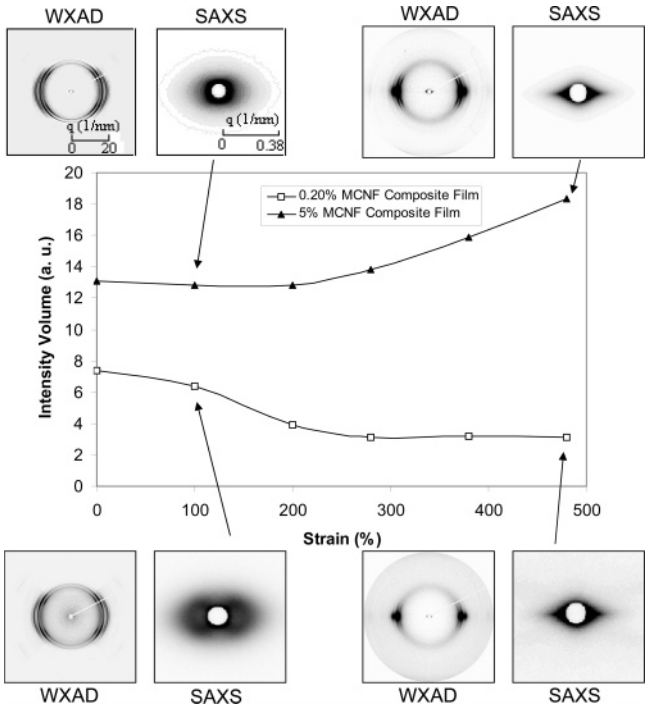


**Figure 9.** Total SAXS intensity changes in MCNF/UHMWPE nanocomposites during stretching at room temperature; also included are selected WAXD and SAXS patterns at strains of 100% and 480%, respectively.

discussion, Figure 8B can also be divided into three regions. Similar trends on the changes in *a*-axis orientation and in *c*-axis orientation are seen in Figure 8B as those in Figure 8A, except for the transition region II which occurs at strain from 300% to 400%. This indicates that the perfection of the *a*-axis orientation and that of the *c*-axis orientation in the 0.2 wt % MCNF film took place earlier than those in the 5 wt % MCNF film during stretching. The final $\bar{P}_2$ value of the *c*-axis orientation in the 5 wt % MCNF sample in region III was found to be lower than that of the 0.2 wt % MCNF sample, indicating that the polyethylene chains orientation in the stretched 5 wt % MCNF sample was less than that of the stretched 0.2 wt % MCNF sample under the same strain. The $\bar{P}_2$ value from the (002) reflection of MCNF was almost the same in regions I and II, and it was very close to 0, indicating that MCNF had very low orientation along the stretching direction at the initial deformation stage. However, the $\bar{P}_2$ value from the (002) reflection of MCNF was found to increase rapidly in region III, similar to the $\bar{P}_2$ values from both (200) reflection of the orthorhombic cell and the ($\bar{2}$10) reflection of the monoclinic cell in this region, even though it had a relatively smaller value. This suggests that MCNF was also orientated along the stretching direction during deformation, but the orientation of MCNF was much lower than that of the polyethylene chains in crystals.

**Small-Angle X-ray Scattering Characterization.** The toughening mechanism in MCNF/UHMWPE nanocomposites can also be probed by in-situ SAXS measurements. Figure 9 illustrates the changes in the integrated SAXS intensity in both nanocomposite samples, which exhibit an opposite trend (one increases with strain while the other decreases) during stretching at room temperature. Selected 2D WAXD/SAXS patterns collected at strains of 100% and 480% are also included in this figure. These results can be explained as follows. It is thought that the measured SAXS intensity contains at least two contributions: (1) the void scattering from CNF (it is known that CNF has a tubelike structure (as seen in Figure 1),[27] which can cause scattering), and (2) the scattering due to the changes in crystallinity. In Figure 9, it is seen that the total intensity in the 5 wt % MCNF film was much higher than that of the 0.2 wt % MCNF film at the initial stage (0% strain), which can be attributed to the larger contribution of the void scattering from MCNF in the 5 wt % sample. For the 0.2 wt % MCNF film, the total intensity was found to decrease rapidly before the strain reached 200% and then reached a plateau value afterward, which was similar to the crystallinity change in Figure 6. This finding makes sense because during stretching, although the MCNF can be reoriented, the SAXS intensity due to the void scattering of CNF is not expected to change. Thus, the decrease in the SAXS intensity in the 0.2 wt % film was mainly due to the crystallinity reduction at the initial stretching stage. For the 5 wt % MCNF film, the total scattering intensity of SAXS was found to increase with strain, which was opposite to the intensity change for the 0.2 wt % MCNF film. Since the crystallinity changes in the two nanocomposite films during stretching were similar (Figure 6), this observation indicates that some other factor must be involved and produce extra scattered intensity in SAXS. We speculate that at high MCNF concentrations the particulate interactions of MCNF became dominant, which could generate additional nanoscale voids in the polymer matrix during deformation, resulting in an increase in the total scattered intensity.

In Figure 9, selected WAXD and SAXS patterns collected at strains of 100% and 480% showed some interesting features. First, the SAXS image for the 0.2 wt % MCNF film at 100% strain exhibited a clear four-point pattern, indicating that a tilted structure was formed with respect to the stretching direction. However, the four-point pattern could not be clearly identified in the SAXS image of the 5 wt % MCNF film, which is consistent with the presence of higher MCNF particulate interactions in the matrix. Second, at 480% strain, SAXS images of both nanocomposite films exhibited an equator streak pattern, indicating an oriented fibrillar structure in the samples. The corresponding WAXD images indicated that the crystal orientation was high. This suggests that the equatorial streak in SAXS may be due to at least two contributions: (1) scattering from noncorrelated fibrillar-like crystal structures and (2) scattering from noncorrelated MCNF; both are aligned with the stretching direction. It was interesting to see that the crystal orientation in the 0.2 wt % MCNF film was higher than that in the 5 wt % MCNF film. This observation again supports the hypothesis of higher particulate interactions in the 5 wt % MCNF film, which hindered the reorganization of the polymer crystals during stretching.

The peculiar SAXS patterns observed at low strains somewhat resemble the "numerical eight" patterns reported by Tsvankin and co-workers[34] and by Stribeck and co-workers.[35] The traditional explanation for this pattern involves the superposition of tilted radial dashes and equatorial arcs. This description can be misleading as it suggests the presence of a heterogeneous system with two qualitatively different regions giving rise to the respective intensity distributions. In this study, the "numerical eight" SAXS pattern can be fully understood

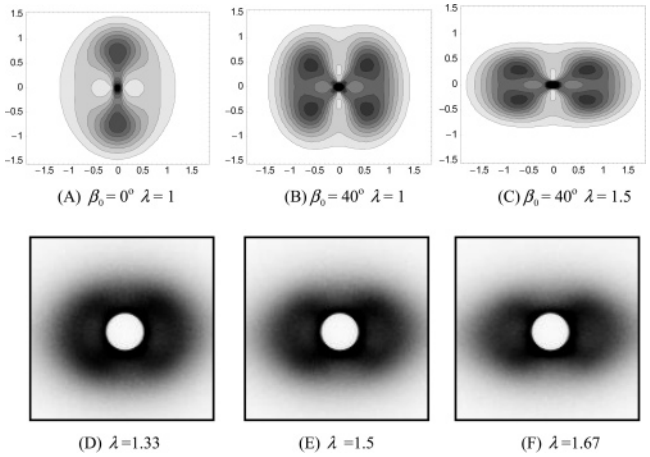


**Figure 10.** Simulated SAXS patterns (A, B and C, Hermans' orientation factor, $\bar{P}_2 = -0.35$, tilt angle $\beta_0$ and stretching factor $\lambda$ as indicated) and experimental SAXS patterns (D, E, and F).

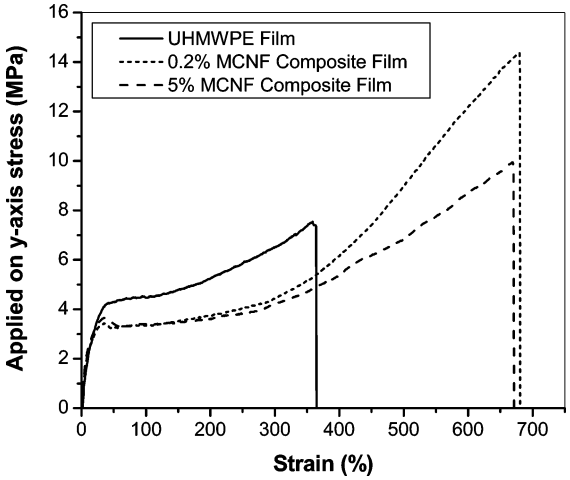


**Figure 11.** Stress−strain curves of the UHMWPE and MCNF/UHMWPE films at 118 °C.

in terms of a single homogeneous system as a consequence of the *a*-axis orientation. Consider a single untilted lamellar stack with the lamella normal pointing in the polymer chain axis direction (*c*-axis of the unit cell), the scattering of which would result in a two-point pattern. In the presence of *a*-axis orientation, this two-point pattern is first rotated about the equatorial axis, leading to a ring, and then rotated about the fiber axis, leading to a ring-shaped scattering pattern with maxima on the meridian (see the simulated SAXS patent in Figure 10A). We note that the nonvanishing intensity on the equator is caused by the averaging of the ring. Tilting the lamellar stack (i.e., tilt angle $\beta_0 = 40°$, which rather means shearing since the *c*-axis of the unit cell does not tilt) leads to the pattern in Figure 10B, exhibiting a tetramodal intensity distribution. Finally, the agreement with the experimental patterns (Figure 10D−F) can be perfected by introducing a stretching deformation (stretching factor $\lambda$), which makes perfect sense for the stretched systems under consideration and leads to quite convincing results (Figure 10C).

**Toughening Performance at High Temperature.** Figure 11 illustrates the stress−strain curves of UHMWPE and MCNF/UHMWPE films at 118 °C. Compared with the stress−strain curves at room temperature, the elongation-to-break ratio of the pure UHMWPE film was found to increase significantly at 118 °C (from

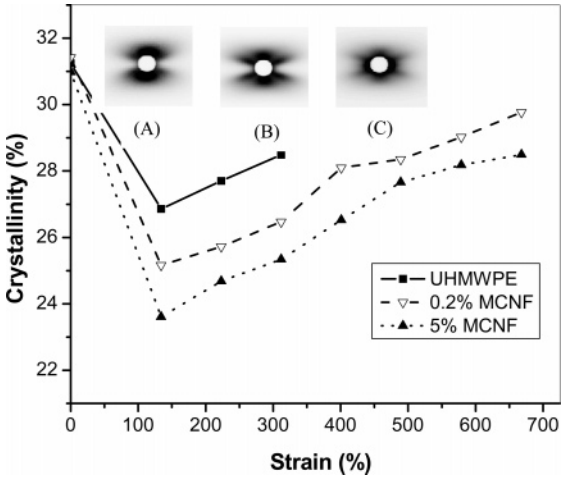


**Figure 12.** Changes of crystallinity for UHMWPE and MCNF/UHMWPE films at 118 °C and different strains. The inset images represent the SAXS patterns of (A) UHMWPE, (B) 0.2 wt % MCNF film, and (C) 5 wt % MCNF film at a strain of 130%.

50% at room temperature to 370%) due to the increased chain mobility at high temperature. The increased chain mobility apparently overcame some entanglement restraints in the UHMWPE matrix. However, the toughness of the MCNF/UHMWPE films was still higher (about 2 times higher) than that of the pure UHMWPE film because of the higher elongation-to-break ratios (ca. 680%, which was about a 20% increase from their room temperature values). The performance of the 0.2 wt % MCNF film was again most interesting, showing not only the highest elongation-to-break ratio but also the highest ultimo-tensile strength. The yield strengths of the nanocomposite films were found to be lower than those of the pure UHMWPE film.

The changes of crystallinity in UHMWPE and MCNF/UHMWPE films at 118 °C during deformation are shown in Figure 12. It was found that the crystallinity decreased abruptly in all samples at the initial stage of deformation (at strains below 130%), indicating that some crystal lamellae were destroyed by stretching, probably through the chain-pulling mechanism. At stains above 130%, the crystallinity was found to increase almost linearly with strain, indicating the reformation of new crystallites (i.e., strain-induced crystallization). These findings have also been observed before by Kanamoto et al.[36] in the two-stage extrusion/drawing study of UHMWPE reactor powder at similar temperatures. In Figure 12, it was found that the reduction of the crystallinity increased with the MCNF content, where the 5 wt % MCNF film exhibited the lowest crystallinity. This may be explained as follows. As the melting point of the pure UHMWPE film (133.6 °C) was the highest among the samples, the average size of the PE crystals in pure UHMWPE film was probably also the largest, which would lead to a more stable crystal structure under deformation. In contrast, the lower melting point in MCNF/UHMWPE suggests the presence of a less stable crystal structure, which could be easily destroyed or altered even under a low deformation strain. This hypothesis was also confirmed by the high-temperature SAXS images collected at strain of 130% (Figure 12). It was seen that the SAXS pattern of the 0.2 wt % film (Figure 12B) clearly exhibited the composite image of a cross pattern along the off-axis and a two-point pattern along the meridian. The cross

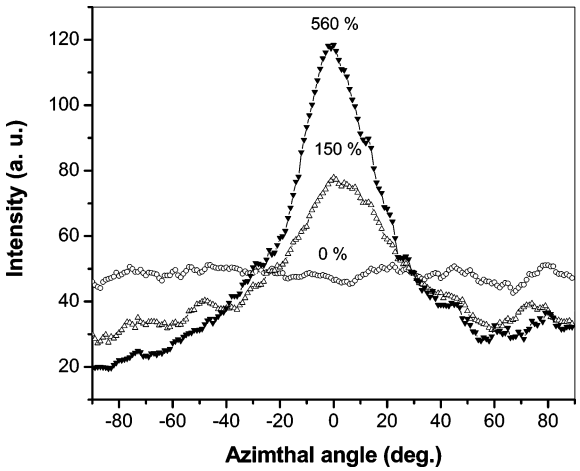


**Figure 13.** Azimuthal intensity profile at the (002) graphite plane ($q = 1.862$ Å$^{-1}$) of MCNF at different strains (from the 2D WAXD patterns of 5 wt % MCNF film).

pattern indicates the presence of a tilted crystal structure, which can be mainly attributed to the reorientation of existing lamellae under deformation. The two-point meridional pattern suggests the presence of a well-aligned lamellar structure with the normal of lamellae parallel to the deformation axis. At high MCNF content (Figure 12C), it appears that the cross pattern became more dominant in SAXS, while the corresponding scattered intensity also became weaker. This suggests that a greater degree of crystal destruction and/or reorientation was achieved in the 5 wt % film under deformation at 118 °C. In contrast, less crystal destruction and/or reorientation was found in the pure UHMWPE film (Figure 12A).

The alignment or orientation of CNFs in the composite film during stretching can be determined by in-situ WAXD measurements. This is because the inner part of the carbon nanofiber wall has an arrangement of graphitic layers at a ±15° angle with respect to the fiber axis, while the outside part of the wall is made up of short graphitic segments parallel to the fiber axis.[9,10] Thus, from the WAXD patterns, the (002) crystal reflection due to the interspacing between the graphite planes in CNFs can be used to characterize the average orientation of CNFs in the composite film. The example azimuthal profiles taken at the (002) CNF reflection ($d = 3.41$Å$^{-1}$) at different strains for the 5 wt % MCNF/UHMWPE sample are shown in Figure 13. It was found that the azimuthal profile of the (002) graphite plane was a flat line when strain was 0, indicating that MCNF was arranged randomly without preferred orientation before stretching. However, upon stretching, the azimuthal profile exhibited a large intensity increase in the equator direction, indicating the realignment of MCNF along the stretching direction. The degree of MCNF orientation was found to increase with the increase in deformation strain. Similar results were also found in in-situ WAXD measurements of 0.2 wt % MCNF/UHMWPE nanocomposites during stretching at room temperature.

Figure 14 shows the integrated SAXS intensity of UHMWPE and MCNF/UHMWPE films during stretching at 118 °C. It was seen that the scattered intensity in the 5 wt % MCNF film was still much higher than that of the 0.2 wt % MCNF film at the initial stage, which was due to larger void scattering from MCNF at high concentrations. The changes of the scattered

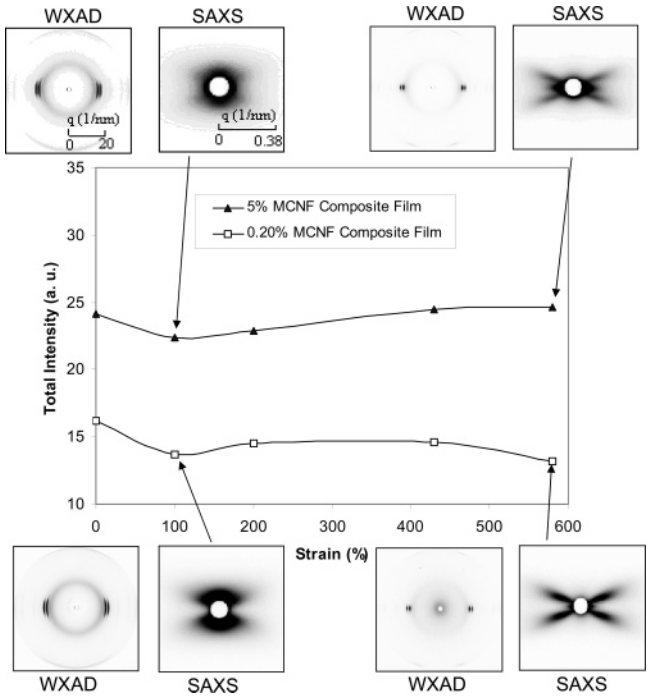


**Figure 14.** Total SAXS intensity changes in MCNF/UHMWPE nanocomposites during stretching at 118 °C; also included are selected WAXD and SAXS patterns at strains of 100% and 580%, respectively.

intensity in both MCNF nanocomposite films exhibited a similar trend. That is the scattered intensity decreased at strains below 100% but increased slightly afterward. This behavior is almost the same as the crystallinity change illustrated in Figure 12, suggesting that the scattered intensity was mainly resulted from the crystallinity change. For the 0.2 wt % MCNF film, the change of the scattered intensity at high temperature was similar to that at room temperature. But for the 5 wt % MCNF film, the behavior was quite different. There appeared to be no excessive void scattering generated from the particulate interactions at high temperature, which could be attributed to a large increase of the chain mobility in the matrix, which minimized the filler effect.

In Figure 14, as the stretching temperature was 118 °C, which was higher than 110 °C, the metastable monoclinic phase was not observed in any of the 2D WAXD patterns. The WAXD images collected at 580% strain showed a highly oriented PE crystal diffraction pattern in both nanocomposite samples. The Hermann orientation factors calculated from the principal crystal diffraction peak (e.g., (110)) in these WAXD images were all approached the value of 1.0, indicating that the crystal orientation in UHMWPE was nearly perfect. The corresponding SAXS images exhibited some interesting patterns. In the 0.2 wt % MCNF film, the SAXS image showed a very strong cross pattern (this is very different from the four-point pattern in Figure 7), superimposed by a weak equatorial streak scattering pattern; while in the 5 wt % MCNF film, the SAXS image showed a composite pattern having strong contributions from both cross and equatorial streak features. As discussed earlier, the equatorial streak scattering can be attributed to two factors: (1) scattering from noncorrelated fibrillar-like crystal structures and (2) scattering from oriented but noncorrelated MCNF. We believe the (2) factor is the dominant one, which would explain the

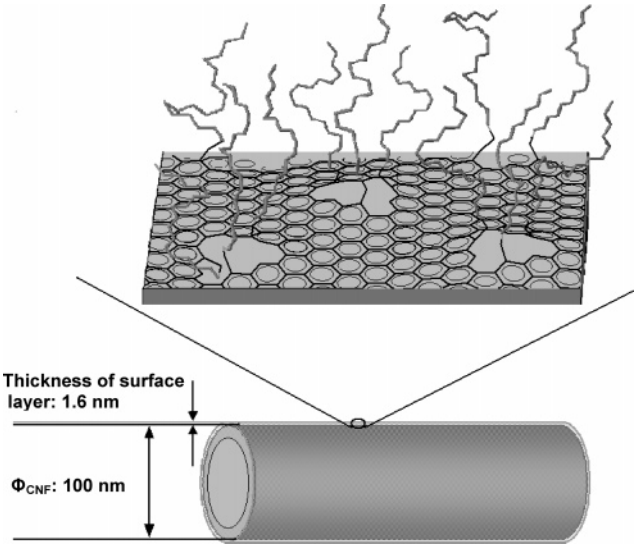


**Figure 15.** Schematic diagram of the interface in MCNF having a layer of oligomeric hydrocarbon chains.

larger fraction of equatorial scattering in the 5 wt % MCNF film. On the other hand, the cross pattern can be attributed to a tilted crystal superstructure containing polymer chains completely parallel to the stretching direction within the crystals (because the Herman orientation factor was about 1). The tilted angle of this crystal superstructure assembly may be caused by the shearing motion during the tensile deformation process. Similar cross patterns were also observed during stretching of UHMWPE gel and PVA gel films by Matsuo et al.[37,38] They found that there was a drastic change in the pattern from the equatorial to meridional direction during deformation, which can be attributed to the crystallization process induced by elongation. However, this kind of drastic change in the scattering pattern was not seen here probably due to the high entanglement of UHMWPE chains, which decreased the elongation of the polymer chain greatly.

**Unique Toughing Mechanism in MCNF/UHMWPE Nanocomposites.** The toughness enhancement in the MCNF/UHMWPE nanocomposite films is very significant at room temperature and also notable at 118 °C. We believe that the unexpected large elongation-to-break ratio (>500% at room temperature) is mainly due to the unique feature of MCNF, where a dense layer of short hydrocarbon chains ($n = 18$) is present on the fiber surface (Figure 15). As these short chains can act as solvent molecules and swell the surrounding polyethylene long chains, a high degree of chain mobility on the MCNF/UHMWPE interface is obtained. It is conceivable that a gel state of UHMWPE/$C_{18}$ is formed on the surface of MCNF, where the range of UHMWPE concentration can be estimated as follows. As the maximum length of the octadecyl group ($n = 18$) on the MCNF surface is about 16 Å [39] (i.e., in the extended crystalline state, which is unlikely), the maximum density of the octadecyl layer is around 60% (assuming the outer diameter of CNF ~ 100 nm and the inner hole diameter of CNF ~ 80 nm, the density of the carbon layer in CNF ~ 2.1 g/cm$^3$, and about every 400 carbon atom had one octadecylamide chain attachment). Thus, the UHMWPE concentration range in the "gel" state of UHMWPE/$C_{18}$ at the MCNF interface should be between 0 and 40 wt %, representing the two limiting UHMWPE concentration values on the MCNF surface.[40] It is imperative to note that as the CNF and the attached $C_{18}$ chains are incompatible, the real UHMWPE concentration at the MCNF/UHMWPE interface will probably be on the high side of the concentration range, but <40 wt %.

At low strains, the mobile interface does not notably affect the overall mechanical properties; but at high strains, the mobile UHMWPE chains at the MCNF interface appears to be critical to overcome the barrier of chain entanglement in the UHMWPE matrix and induces plastic flow on a macroscopic scale. It can be envisioned that the interfacial flow in the vicinity of MCNF can (1) orient the alignment of MCNF and (2) cause the polymer chain extension, resulting in a significant increase in the elongation-to-break ratio, as well as the strain hardening behavior in nanocomposites (see Figures 4 and 11). It is interesting to note that at high strains the mechanical properties of the 0.2 wt % MCNF film are superior to those of the 5 wt % MCNF film. This behavior can be explained by the filler interactions at higher concentrations, which hinder the extension of polymer chains near the interface.

## Conclusions

In summary, the surface modification of carbon nanofibers with octadecylamide groups (short hydrocarbon chains with $n = 18$) could serve as a solvent carrier to soften the very stiff UHMWPE matrix. In addition, the surface modification could also significantly facilitate the dispersion and improve the surface adhesion of MCNF in UHMWPE during melt processing. The nanocomposite film having only a small amount of MCNF (e.g., 0.2 wt %) showed a significant improvement on the elongation-to-break ratio and, thus, the toughness in both room temperature and high temperature (118 °C). The MCNF/UHMWPE sample thus represents a new type of nanocomposite with enhanced toughening performance. The use of unmodified CNF also exhibited improvement on the toughness, but way below the level found in MCNF/UHMWPE. The significantly toughened performance of the MCNF/UHMWPE nanocomposite film is related to the interfacial flow of the UHMWPE chains. As the attached octadecylamide groups act as solvent molecules to UHMWPE, the gel-like UHMWPE/$C_{18}$ layer can overcome the high entanglement restraints (thus the brittleness) in solid UHMWPE. In-situ synchrotron WAXD/SAXS measurements showed that although the increase in MCNF content induced a higher degree of plastic flow, the increase in particulate interactions also decreased the elongation-to-break ratio. The optimal toughness improvement occurred at a very low concentration of MCNF incorporation in UHMWPE.

**Acknowledgment.** The financial support of this work was provided by the Department of Energy (DEFG0286ER45237.022 and DEFG0299ER45760), the Office of Naval Research (N000140310932), and the National Science Foundation (DMR0405432 and DMR0098104). The authors acknowledge a helpful discussion with Prof. Paul Smith of ETH for the possible toughening mechanism of the MCNF/UHMWPE nanocomposites.

## References and Notes

(1) Iijima, S. *Nature (London)* **1991**, *354*, 56.
(2) Haddon, R. C. *Acc. Chem. Res.* **2002**, *35*, 997.

(3) Che, G.; Lakshmi, B. B.; Martin, C. R.; Fisher, E. R. *Chem. Mater.* **1998**, *10*, 260.
(4) Hone, J.; Batlogg, B.; Benes, Z.; Johnson, A. T.; Fischer, J. E. *Science* **2000**, *289*, 1730.
(5) Wagner, H. D.; Lourie, O.; Feldman, Y.; Tenne, R. *Appl. Phys. Lett.* **1998**, *72*, 188.
(6) Qian, D.; Dickey, E. C. *Appl. Phys. Lett.* **2000**, *76*, 2868.
(7) Ruan, S. L.; Gao, P.; Yang, X. G.; Yu, T. X. *Polymer* **2003**, *44*, 5643.
(8) Finegan, I. C.; Tibbetts, G. G.; Glasgow, D. G.; Ting, J. M.; Lake, M. L. *J. Mater. Sci.* **2003**, *38*, 3485.
(9) Ma, H.; Zeng, J.; Realff, M. L.; Kumar, S.; Schiraldi, D. A. *Compos. Sci. Technol.* **2003**, *63*, 1617.
(10) Sandler, J.; Windle, A. H.; Werner, P.; Altstadt, V.; Es, M. V.; Shaffer, M. S. P. *J. Mater. Sci.* **2003**, *38*, 2135.
(11) Bin, Y.; Kitanaka, M.; Zhu, D.; Matsuo, M. *Macromolecules* **2003**, *36*, 6213.
(12) Dalton, A. B.; Collins, S.; Munoz, E.; Razal, J. M.; Ebron, V. H.; Ferraris, J. P.; Coleman, J. N.; Kim, B. G.; Baughman, R. H. *Nature (London)* **2003**, *423*, 703.
(13) Rodriguez, N. M. *J. Mater. Res.* **1993**, *8*, 3233.
(14) Pennings, A. J.; Smook, J.; de Boer, J.; Gogolewski, S.; van Hutten, F. F. *Pure Appl. Chem.* **1983**, *55*, 777.
(15) Smith, P.; Lemstra, P. *J. Colloid Polym. Sci.* **1980**, *258*, 891.
(16) Kanamoto, T.; Tsuruta, A.; Tanaka, K.; Takeda, M.; Porter, R. S. *Macromolecules* **1988**, *21*, 470.
(17) Hoogsteen, W.; van der Hooft, R. J.; Postema, A. R.; ten Brinke, D.; Pennings, A. J. *J. Mater. Sci.* **1988**, *23*, 3459.
(18) Nakae, M.; Uehara, H.; Kanamoto, T.; Zachariades, A. E.; Porter, R. S. *Macromolecules* **2000**, *33*, 2632.
(19) Uehara, H.; Nakae, M.; Kanamoto, T.; Zachariades, A. E.; Porter, R. S. *Macromolecules* **1999**, *32*, 2761.
(20) Friend, S. O.; Barber, J. J. U.S. Patent # 5611964, 1997.
(21) Hu, H.; Bhowmik, P.; Zhao, B.; Hamon, M. A.; Itkis, M. E.; Haddon, R. C. *Chem. Phys. Lett.* **2001**, *345*, 25−28.
(22) Wunderlich, B.; Cormier, C M. *J. Polym. Sci., Polym. Part A-2* **1967**, *5*, 987.
(23) Chu, B.; Hsiao, B. S. *Chem. Rev.* **2001**, *101*, 1727.
(24) Ran, S.; Wang, Z.; Burger, C.; Chu, B.; Hsiao, B. S. *Macromolecules* **2002**, *35*, 10102.
(25) Calculated based on the measured mole ratio of COOH group and the number of carbon atoms in 1 g of CNF.
(26) Based on the properties of Pyrograf®-III and Pyrograf®-I given by the Applied Sci. Inc. (http://www.apsci.com/ppi-pyro3.html; http://www.apsci.com/ngm-pyro1.html).
(27) Sakurada, I.; Ito, T.; Nakamae, K. *J. Polym. Sci.* **1966**, *15*, 75.
(28) Wilkes, G. L. Mechanical Properties. In *Comprehensive Desk Reference of Polymer Characterization and Analysis;* Brady, R. F., Jr., Ed.; Oxford University Press: New York, 2003; p 624.
(29) Russell, K. E.; Hunter, B. K.; Heyding, R. D. *Polymer* **1997**, *38*, 1409.
(30) Butler, M. F.; Donald, A. M.; Bras, W.; Mant, G. R.; Derbyshire, G. E.; Ryan, A. J. *Macromolecules* **1995**, *28*, 6383.
(31) Teare, P. W.; Holmes, D. R. *J. Polym. Sci.* **1957**, *24*, 496.
(32) Bevis, M.; Crellin, E. B. *Polymer* **1971**, *12*, 666.
(33) Aggarwal, S. L.; Tilley, G. P.; Sweeting, O. J. *J. Polym. Sci.* **1961**, *51*, 551.
(34) Gerasimov, V. I.; Genin, Ya. V.; Tsvankin, D. Ya. *J. Polym. Sci., Polym. Phys. Ed.* **1974**, *12*, 2035.
(35) Androsch, R.; Stribeck, N.; Lupke, T.; Funari, S. S. *J. Polym. Sci., Part B: Polym. Phys.* **2002**, *40*, 1919.
(36) Kanamoto, T.; Ohama, T.; Tanaka, K.; Takeda, M.; Porter, R. S. *Polymer* **1987**, *28*, 1517.
(37) Matsuo, M.; Inoue, Y.; Abumiya, N. *Seni-Gakaishi* **1984**, *40*, 275.
(38) Sawatari, C.; Yamamoto, Y.; Yanagida, N.; Matsuo, M. *Polymer* **1993**, *34*, 956.
(39) The maximum chain distance ($L$) of the octadecylamide group was calculated by using $L = nl\cos(\theta/2)$, where the attached group was assumed to crystallize into an extended state $n = 18$, $l = 0.154$ nm, and $\theta = 109.5°$.
(40) 40 wt % is the estimated maximum UHMWPE concentration in the MCNF/UHMWPE gel at the surface of MCNF, corresponding to the UHMWPE concentration at the outer rim of MCNF when the attached octadecylamide chain ($n = 18$) is fully extended; 0 wt % is the minimum UHMWPE concentration, corresponding to the concentration at the interface which is entirely occupied by the octadecylamide chains.

MA047978R